THE JOURNAL OF PHYSICAL CHEMISTRY C

Article

pubs.acs.org/JPCC

Role of Interface in the Lithiation of Silicon-Graphene Composites: A First Principles Study

Chia-Yun Chou[†] and Gyeong S. Hwang*[,†,‡]

[†]Materials Science and Engineering Program and [‡]Department of Chemical Engineering, University of Texas at Austin, Austin, Texas 78712, United States

ABSTRACT: We examine the lithiation behavior of silicon-graphene (Si-Gr) composites using density functional theory calculations. Our calculations demonstrate charge transfer from Li to both Si and C (in graphene); the excess electrons on graphene create an electric field, which attracts Li cations while repelling Si anions and thus results in a distinct alternative Li−Si layering structure near graphene. The interfacial Li ions exhibit substantially higher mobility along the Si/Gr interface in comparison to bulk diffusion in Si; such facile interfacial diffusion could contribute toward high performance anodes with fast charge/discharge rates. However, the presence of graphene tends to have no significant impact on the structural evolution of Si during lithiation, as Li atoms are mostly incorporated in the Si matrix rather than at the Si/Gr interface. Consequently, the theoretical capacity and voltage profile of the Si-Gr composite are predicted to be close to those of pure Si.

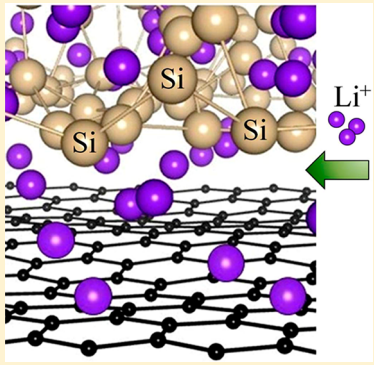

1. INTRODUCTION

Facing the ever-increasing demand for safer lithium (Li) ion batteries (LIBs) with high energy density, rapid charge rate, and long cycle life, there is an urgent need to find a new electrode material in replacing graphite which has a limited theoretical capacity of 372 mAh/g (LiC_6). Among the alternative anode materials considered, silicon (Si) stands out the most because of its highest known theoretical capacity about 4200 mAh/g ($Li_{4.4}Si$)[1,2] and abundance. However, the practical use of Si as an anode material is hampered by its large volume expansion, causing pulverization, loss of electrical contact, and consequently early capacity fading. For this reason, considerable efforts have been made to overcome these drawbacks, including structural modifications such as utilizing amorphous phases,[3−5] nanoparticles[6,7] and nanowires,[8] and alloying Si with active/inactive elements.[9−12]

Nanostructured Si in particular has shown promising improvements, as it can accommodate larger strain and provide better mechanical integrity since its dimension would limit the size and propagation of cracks.[13−15] By combining Si with carbonaceous (C) materials (Si−C), the cycling stability can be further improved with the enhanced buffering effect and electrical conductivity from carbon.[16−23] Several structurally superior designs have been demonstrated by researchers, including (1) making nanosized Si−C composites in particular forms such as core−shell heterostructures;[16,19] (2) depositing Si−C multilayer films;[24] (3) making Si-graphene composites by coating Si on graphene[25] or encapsulating Si nanoparticles with crumpled graphene;[26,27] and (4) putting C coating on Si nanowires or coating tubular forms of C with Si.[17,18,20−23] As the result, excellent capacity retention was realized by composites made of Si and carbonaceous materials; nano-silicon-coated graphene granules have been reported with capacity exceeding 2000 mAh/g at the current density of 140 mA/g and excellent stability for 150 cycles,[25] and near-theoretical capacity (of Si) could be achieved (3890 mAgh/g) for more than 100 cycles in Si−C thin films, which is thought to be attributed to the buffering effect of intercalated C layers.[24] Furthermore, nanostructured Si−C anodes have also been utilized to enhance the high-rate capabilities; previously, capacity as high as 2000 mAh/g was reported at 5C charging rate (full lithiation in 1/5 h) for Si decorated carbon nanotubes,[28] and capacity in excess of 1500 mAh/g was demonstrated at 8C rate using porous Si−C composites.[29]

As a promising anode material for LIBs, Si−C composites exhibit many unique synergistic benefits, such as remarkable capacity retention and rate capabilities. However, in comparison to pure Si or C anodes, it is more challenging to investigate the lithiation behavior in Si−C composite anodes, especially concerning the complexities and intricate reactions at Si/C interfaces. On the theoretical side, there have been many studies employing density functional theory (DFT) to examine Li incorporation in Si (crystalline/amorphous bulks[30−33] and NWs[34−36]), graphite,[37,38] and graphene.[39−43] However, to the best of our knowledge, no atomistic-scale study has been reported regarding the lithiation behavior in Si−C composites.

In this paper, based on DFT calculations we present the structural evolution and voltage profile of the lithiated Si-graphene (Si-Gr) composite, and also discuss the bonding mechanism and Li diffusivity in Li_xSi-Gr systems ($0 \leq x \leq 4.33$), with particular attention to the effect of the Si/Gr interface. In reality, Si−C composites could be composed of Si

Received: March 8, 2013
Revised: April 19, 2013
Published: April 22, 2013

with graphite (or multiple layers of graphene) or turbostratic carbon (disordered graphite); however, most of the constituent C atoms are likely sp^2 bonded, so it would be reasonable to use the Si-Gr model structure for investigating the Si/C interface effect. The fundamental findings from this computational work will contribute to a better understanding of the properties and performance of Si−C nanocomposites as LIB anode materials.

2. COMPUTATIONAL METHOD

The calculations reported herein were performed based on DFT within the generalized gradient approximation (GGA-PW91),[44] as implemented in the Vienna Ab-initio Simulation Package (VASP).[45−47] The projected augmented wave (PAW) method with a plane-wave basis set was employed to describe the interaction between ion core and valence electrons. The PAW method is in principle an all-electron frozen-core approach that considers exact valence wave functions. Valence configurations employed are as follows: $1s^2 2s^1$ for Li, $3s^2 3p^2$ for Si, and $2s^2 2p^2$ for C. An energy cutoff of 400 eV was applied for the plane-wave expansion of the electronic eigenfunctions.

As illustrated in Figure 1, each Li_xSi-Gr supercell consists of a 48-atom 12.8187 × 9.8680 Å^2 rectangular graphene sheet which

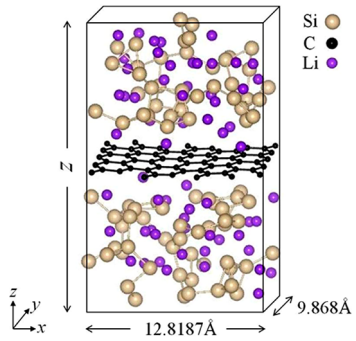

Figure 1. Side view of a Li_xSi-Gr system in which the *a*-Li_xSi alloy is interfaced with a 48-atom rectangular graphene sheet (12.8187 × 9.8680 Å^2). The *z*-dimension values are summarized in Table 1.

is interfaced with the amorphous Li_xSi alloy (*a*-Li_xSi) of desired composition (*x* varies from 0 to 4.33).

Here, we used the GGA-optimized lattice constant of 2.467 Å for graphene, which is in good agreement with the experimental value of 2.46 Å.[48] The compositions and dimensions of the Li_xSi-Gr systems considered are summarized in Table 1.

The model structures for bulk *a*-Li_xSi alloys were created based on ab initio molecular dynamics (AIMD) simulations as previously described in ref 49. To simulate a Li_xSi-Gr system, the *a*-Li_xSi bulk alloy and graphene sheet were placed approximately 2 Å apart and fully relaxed using a conjugate gradient method until residual forces on constituent atoms became smaller than 5×10^{-2} eV/Å. The Li_xSi-Gr system was then annealed at 500 K for 1 *ps* with a time step of 1 *fs* to allow sufficient atomic rearrangement (the annealing temperature was controlled via velocity rescaling), followed by geometry optimization. For geometry optimization, the Brillouin zone sampling was done with a Γ-centered (2 × 2 × 1) Mockhorst-Pack grids,[50] and for charge analysis an increased *k*-point mesh size (6 × 6 × 1) was used to refine the calculations. Periodic boundary conditions were employed in all three directions, and for each composition three independent samples were considered. AIMD simulations of 18 *ps* duration with a time step of 1 *fs* were carried out at 800 K (temperature was controlled via Nosé-Hoover thermostat) to calculate Li diffusivities in $Li_{1.0}Si$-Gr and the counter bulk *a*-Li_xSi alloy.

Table 1. Compositions of the Li_xSi-Gr Systems Employed in This Work, Together with the *z*-Dimension Values which Are Averaged Based on Three Different Supercells (See Figure 1 for a Schematic of the Supercell)

x in Li_xSi-Gr (# Li/Si/C)	*z*-Dimension (Å)
0.00 (0/64/48)	16.26 ± 0.32
0.13 (8/64/48)	16.64 ± 0.27
0.25 (16/64/48)	17.35 ± 0.35
0.50 (32/64/48)	18.52 ± 0.31
0.75 (48/64/48)	19.87 ± 0.31
1.00 (64/64/48)	21.24 ± 0.09
1.67 (80/48/48)	20.70 ± 0.58
2.35 (90/38/48)	20.65 ± 0.13
3.57 (100/28/48)	20.44 ± 0.21
4.33 (104/24/48)	20.82 ± 0.11

3. RESULTS AND DISCUSSION

3.1. Atomic Arrangement and Bonding Mechanism near the Lithiated Si/Gr Interface. First, we examined the lithiated structures of the Si-Gr composite with varying Li contents. Figure 2 shows a set of atomic structures from our simulations for selected Li_xSi-Gr systems (*x* = 1.00, 1.67, and 3.57).

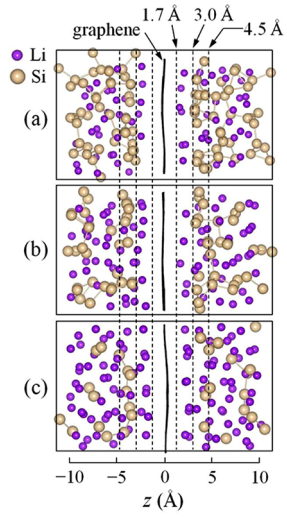

Figure 2. Set of atomic structures from our simulations for (a) $Li_{1.00}Si$-Gr, (b) $Li_{1.67}Si$-Gr, and (c) $Li_{3.57}Si$-Gr. The graphene position is set to zero (in *z*-dimension).

We notice a distinct Li enrichment at the Li_xSi/Gr interface, but away from the graphene layer, Li and Si atoms tend to be well-mixed similar to bulk Li_xSi alloys.[49] As partitioned by the vertical dashed lines, away from graphene (|*z*| = 0.0 Å), the first layer (|*z*| ≈ 1.7 to 3.0 Å) comprises only Li atoms with the average Li-Gr distance around 2.3 Å, the second layer (|*z*| ≈ 3.0 to 4.5 Å) is mainly composed of Si atoms while the third layer consists of a blend of Li and Si atoms but slightly richer in Li. The distinct layering near graphene tends to be pertinent within the first two to three atomic layers. Further away from graphene, the bulk-like structure is restored where Li and Si atoms are well mixed without segregation.[49]

dx.doi.org/10.1021/jp402368k | J. Phys. Chem. C 2013, 117, 9598−9604

As summarized in Table 2, our results from Bader charge analysis[51] suggest the charge transfer from Li to both Si and C (in graphene), which is not surprising considering their relative electronegativity values (χ_{Li} = 0.98, χ_{Si} = 1.90, and χ_C = 2.55).

Table 2. Calculated Bader Charges for C (in Graphene), Li, and Si Atoms in Selected Li_xSi-Gr Systems

x	C	Li	Si
1.00	−0.07 ± 0.01	+0.85 ± 0.00	−1.49 ∼ −0.22
1.67	−0.08 ± 0.01	+0.83 ± 0.00	−2.30 ∼ −0.59
3.57	−0.13 ± 0.00	+0.80 ± 0.01	−3.32 ∼ −1.58

The C atoms are more negatively charged with increasing Li content (x), while the Li charge state remains nearly constant, and the Si charge state varies significantly depending on the Si−Si connectivity.[49] As such, it is apparent that the alternative layering of Li and Si is due to the electrostatic interaction between them; that is, the excess negative charges on graphene create an electric field, which attracts Li^+ counterions while repelling Si^- co-ions to screen the field, as illustrated in Figure 3.

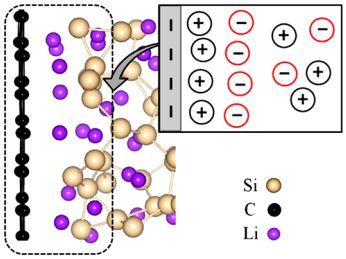

Figure 3. Illustration of how Li cations and Si anions are distributed near negatively charged graphene due to the electrostatic interactions between them.

With increasing Li content, we see a rise in excess negative charges on graphene, which in turn causes more Li cations accumulating at the interface. Also note here, Li atoms are randomly dispersed across the graphene surface rather than each locating on top of the C hexagonal (as seen in the case of single Li adsorption on graphene[37,40]). This difference together with the aforementioned larger Li-Gr distance of ∼2.3 Å (as compared to 1.73 Å for single Li adsorption on graphene) suggest that the interaction of Li with graphene in Li_xSi-Gr systems is somewhat weaker than that in the Li-Gr case; this can be attributed to the additional interaction between the Li and Si layers.

For a better understanding of the interfacial interaction, we conducted more detailed analysis of atomic arrangement, charge transfer, and charge distribution in the $Li_{1.0}Si$-Gr system. Figure 4a presents the number density, $\langle\rho_N\rangle$, profiles of Li and Si along the direction normal to the graphene surface, which clearly demonstrates their alternative layering near graphene.

All the results are averaged (denoted by angular bracket) based on three different samples. As shown in the inset of Figure 4, the corresponding charge redistribution is quantified by the charge-density difference ($\Delta\rho$), which is obtained by subtracting the charge densities of isolated Li, Si, and graphene from that of $Li_{1.0}Si$-G (i.e., $\Delta\rho = \rho[Li_{1.0}Si\text{-}Gr] - \rho[Li] - \rho[Si] - \rho[Gr]$). The $\Delta\rho$ plot illustrates the excess electron accumulation on graphene with an appreciable polarization toward Li cations, which suggests a dominant ionic bonding

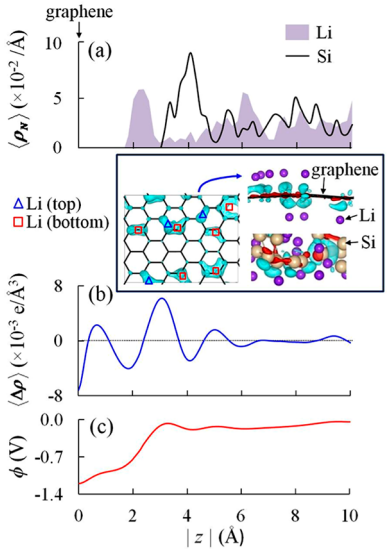

Figure 4. (a) Number density $\langle\rho_N\rangle$ profiles of Li and Si atoms along the z-axis near graphene (located at $|z| = 0$) in $Li_{1.0}Si$-Gr. (b) Planar (x−y plane) averaged charge density difference $\langle\Delta\rho\rangle$ profile. (c) Electric-potential (ϕ) profile with respect to the bulk potential (ϕ = 0 V). The inset shows the charge density difference ($\Delta\rho$) due to Li−Gr and Li−Si interactions, together with the corresponding Li ion positions (on top and bottom sides of the graphene sheet). The cyan (gray) and red (black) isosurfaces represent the regions of charge gain (Li−Gr: +0.0035 e/Å^3 and Li−Si: +0.055 e/Å^3) and charge loss (Li−Gr: −0.0019 e/Å^3 and Li−Si: −0.006 e/Å^3), respectively.

character. Perturbed by the electrostatic interaction with Li ions, significant charge redistribution also occurs within the graphene layer, leading to electron puddles (with some electron depletion in the C−C bonds) in the vicinity of Li atoms. Similarly, the excess electron charge on Si also exhibits noticeable polarization toward Li (along with slight charge depletion in the Si−Si bonds), indicating that the Li−Si bonding is predominantly ionic.

The charge density difference averaged over the x−y plane, $\langle\Delta\rho\rangle$, as a function of $|z|$ is shown in Figure 4b with the position of the graphene sheet set at $|z| = 0$ Å. The $\langle\Delta\rho\rangle$ profile fluctuates extensively near graphene and gradually dampens till nearly flat in the bulk region. The positive$\langle\Delta\rho\rangle$ humps around 0.6 Å and 3.0 Å correspond to electron gain in the graphene and Si layers, respectively; notice that both humps deviate slightly from their corresponding atomic positions ($\langle\rho_N\rangle$ peak positions) with a shift toward the Li layer, as indicative of the appreciable polarization due to the electrostatic interaction with the Li layer.

As demonstrated earlier, the excess electrons on graphene create an electric field (E_{ES}) that causes the redistribution of Li and Si ions, which in turn gives rise to a charge imbalance at the $Li_{1.0}Si$/Gr interface. The resulting electric-potential (ϕ) profile along the direction normal to the graphene surface is obtained by solving Poisson's equation:

$$\nabla^2\phi(z) = \langle\Delta\rho(z)\rangle/\varepsilon_0 \quad \text{with} \quad -\nabla\phi|_{ES} = E_{ES} \qquad (1)$$

where z is the distance from the graphene plane, $\langle\Delta\rho\rangle$ is the x−y planar averaged charge-density difference, and ε_0 is the vacuum permittivity. By integrating eq 1, we can evaluate the potential variation near the $Li_{1.0}Si$/Gr interface:

dx.doi.org/10.1021/jp402368k | J. Phys. Chem. C 2013, 117, 9598−9604

$$\phi(z) = -\frac{1}{\varepsilon_0}\int_0^z (z - z')\langle \Delta\rho(z')\rangle \, dz' \quad (2)$$

Figure 4c shows a calculated potential profile (with a bin size of 0.1 Å)[52] near the graphene plane with respect to the bulk potential (which is set equal to 0 V). The result shows that the potential drops rapidly across the first Li layer, indicating that the accumulated Li counterions effectively screen E_{ES}.

3.2. Interface Effect on Li Diffusion. To examine how the presence of graphene affects Li diffusion, we calculated the diffusivity of Li near graphene, in comparison to the corresponding *a*-Li_xSi bulk alloy. Figure 5 shows the total

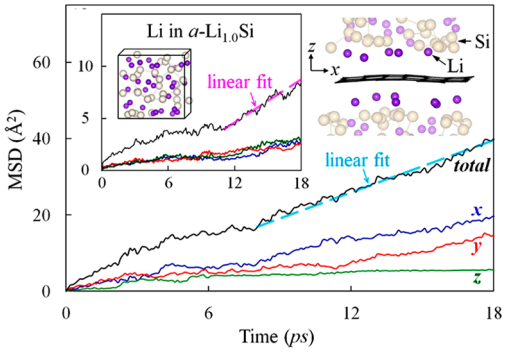

Figure 5. Total and decomposed mean squared displacement (MSD) profiles in *x*, *y*, and *z*-directions for Li atoms near graphene (in $Li_{1.0}Si$-Gr) at 800 K. For comparison, the MSD profiles for Li atoms in bulk *a*-$Li_{1.0}Si$ are also presented in the inset.

and decomposed (in *x*, *y*, and *z*-directions) mean-square displacement (MSD) profiles for Li atoms near graphene in the $Li_{1.0}Si$-Gr system from AIMD simulations; MSD = $|R_i(t) - R_i(0)|^2$, where $R_i(t)$ is the position of atom *i* at time *t*. For comparison, the MSD profiles for Li atoms in bulk *a*-$Li_{1.0}Si$ are also shown in the inset.

At 800 K, the AIMD duration of 18 ps (*ps*) appears to be sufficient as the MSDs of Li atoms in both $Li_{1.0}Si$-Gr and *a*-$Li_{1.0}Si$ were well converged after 9 and 12 *ps*, respectively. For Li atoms in *a*-$Li_{1.0}Si$, the decomposed MSD profiles are compatible in all three directions, indicating the movements of Li atoms are isotropic as expected. Contrarily, Li atoms near graphene (in the $Li_{1.0}Si$-Gr system) exhibit very different diffusion behavior; the MSDs in *x*- and *y*-directions increase progressively at compatible rates while the MSD value in the *z*-direction is negligible. This finding provides a clear picture that Li diffusion near graphene is two-dimensional parallel to the graphene sheet. Once MSD profiles are well converged, corresponding Li diffusivities can be obtained using the Einstein relation, $D = \langle MSD\rangle/(nt)$ with $n = 6$ (4) for three (two)-dimensional diffusion; the angular bracket denotes an ensemble average over the AIMD interval. Disregarding the first few picoseconds, as illustrated in Figure 5, a linear fit over the time interval yields $D_{Li} = (4.74 \pm 0.60) \times 10^{-5}$ cm^2/s near graphene in the $Li_{1.0}Si$-Gr system, which is about five times greater than $D_{Li} = (1.02 \pm 0.40) \times 10^{-5}$ cm^2/s in the counter bulk alloy at 800 K. Our results suggest that D_{Li} can be substantially enhanced in Si−C nanocomposites due to facile diffusion along the Si/C interface, which is consistent with previous experimental observations that show significantly improved lithiation rates in Si−C composite systems.[17,53]

3.3. Energetics and Structural Evolution of Lithiated Si-Gr Systems. We calculated the relative formation energies of the Li_xSi-Gr systems as a function of Li content ($0 \le x \le 4.33$), with respect to crystalline Si (*c*-Si), body-centered cubic Li (*bcc*-Li), and free-standing graphene (Gr). Here, the formation energy per Si atom (E_f) is given by

$$E_f = (E_{Li_xSi-Gr} - E_{Gr})/N_{Si} - (xE_{Li} + E_{Si}) \quad (3)$$

where E_{Li_xSi-Gr} and E_{Gr} are the total energies of the Li_xSi-Gr system and free-standing graphene, respectively, N_{Si} is the number of Si atoms, *x* is the Li content per Si, and E_{Li} and E_{Si} are the per-atom energies of *bcc*-Li and *c*-Si, respectively.

As shown in Figure 6a, the calculated E_f decreases monotonically with increasing *x* and approaches a minimum

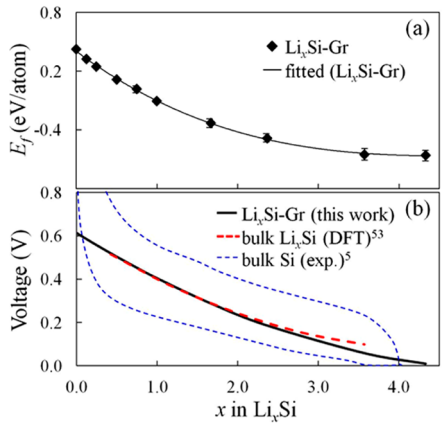

Figure 6. (a) Formation energies (E_f) for Li_xSi-Gr ($0 \le x \le 4.33$) calculated based on three different samples for each composition. (b) Voltage−composition (V−x) curve for lithiated Si-Gr in comparison to that of pure Si.

value around $x = 4$. During early stages of lithiation, Li atoms are preferably accommodated near graphene, and as *x* continues to increase more Li atoms are further dispersed into the Si bulk region forming well mixed Li−Si alloys. Reaching the minimum-energy "plateau" around $x = 4$ implies that the Li_xSi/G system is fully lithiated. The predicted capacity is close to that of pure Si, which is consistent with previous experiments that demonstrate a high Li storage capacity of 3890 mAh/g in Si/C films ($\sim Li_4Si/C$).[24] Our results suggest the presence of graphene has a negligible impact on Li incorporation in the Si matrix, which is not surprising considering the extent of Li_xSi/Gr interface effect is predicted to be very shallow.

Based on the calculated E_f profile, the voltage-composition (V−x) curve for the lithiated Si-Gr system was obtained by

$$V = -dE_f(x)/dx \quad (5)$$

Taking the negative of the derivative of the third order polynomial fittings according to eq 5, the V−x curve of lithiated Si-Gr with comparison to that of bulk Si is shown in Figure 6b. The curves turn out to overlap each other almost in the entire composition range, showing the Si-Gr lithiation voltage profile is nearly the same as the case of pure Si. Such a similarity is reasonable, because given the C:Si atomic ratio in the Li_xSi-Gr system considered, the majority of Li atoms are incorporated in the Si matrix rather than at the Li_xSi/Gr interface, and thus the voltage profile is dominated by Si lithiation.

Next, the structural evolution of selected Li_xSi-Gr systems (x = 1.00, 1.67, and 3.57) was analyzed in terms of Si coordination

dx.doi.org/10.1021/jp402368k | J. Phys. Chem. C 2013, 117, 9598−9604

Table 3. Coordination Statistics (C_n in %, where $n = CN_{Si-Si}$) for Si Networks in Selected Li_xSi-Gr Systems (x = 1.00, 1.67, and 3.57) and Corresponding Bulk a-Li_xSi Alloys for Comparison (In Parentheses)

	C_n (Si−Si)		
n	x = 1.00	x = 1.67	x = 3.57
0			32.1 ± 9.4 (40.5 ± 4.1)
1	3.1 ± 1.6	19.4 ± 3.2 (18.8 ± 2.9)	52.4 ± 16.5 (42.9 ± 0.0)
2	35.9 ± 5.4 (35.4 ± 11.0)	49.3 ± 6.7 (58.3 ± 11.8)	15.5 ± 7.4 (16.7 ± 4.1)
3	49.0 ± 3.9 (54.2 ± 15.7)	29.9 ± 7.3 (22.9 ± 8.8)	
4	12.0 ± 1.8 (10.4 ± 4.8)	1.4 ± 1.2	

number (CN_{Si-Si}). According to the results summarized in Table 3, upon lithiation, the connectivity of Si network (in Li_xSi-Gr) decreases following the general Zintl rule as also seen in the counter bulk Li_xSi alloys.[49,54]

Figure 7 shows the variation in CN_{Si-Si} along the direction normal to the graphene surface. For $Li_{1.0}Si$-Gr, the average

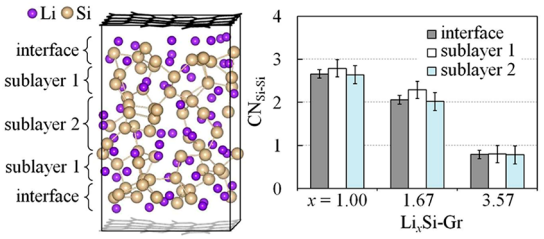

Figure 7. Side view of a sample Li_xSi-Gr supercell divided into the interface layer and two sublayers of equal-thickness (as indicated by interface, sublayer1, and sublayer2, respectively). The histograms (right panel) show variations in CN_{Si-Si} along the direction normal to graphene surface in selected Li_xS-Gr systems (x = 1.00, 1.67, and 3.57).

CN_{Si-Si} values are around 2.7 in all three layers, and with further increase in Li content, CN_{Si-Si} drop to 2.1 in $Li_{1.67}Si$-Gr and 0.8 in $Li_{3.57}Si$-Gr. There is no significant deviation in CN_{Si-Si} values crossing different layers, which confirms the shallow Li_xSi/Gr interface effect as aforementioned.

4. CONCLUSIONS

DFT calculations were performed to examine the atomic arrangement, bonding mechanism, Li diffusion, and lithiation energetics in the Li_xSi-Gr systems (x = 0 to 4.33). Our simulations predict a unique alternative Li−Si layering structure near graphene, due to the electrostatic interactions between positively charged Li and negatively charged Si and graphene. Such layering is found to extend about 2−3 atomic layers, beyond which uniform mixing is restored as in bulk a-Li_xSi alloys. The average Li-Gr distance in selected Li_xSi-Gr systems (x = 1.00, 1.67, and 3.57) is around 2.3 Å, which is larger than 1.73 Å as estimated for single Li adsorption on free-standing graphene; this may suggest the interaction of Li with graphene in the Li_xSi-Gr system is relatively weaker than that in the Li-Gr case, due to the additional interaction with Si. We also examined the effect of graphene on Li diffusion via AIMD simulations; for $Li_{1.0}Si$-Gr at 800 K, the Li diffusivity near graphene is predicted to be approximately five times larger than that in the bulk a-$Li_{1.0}Si$ alloy. We expect that such a significant enhancement in Li mobility could contribute toward high performance anodes with fast charge/discharge rates. Moreover, our calculations demonstrate that during lithiation Li atoms are mainly incorporated in the Si matrix rather than at the Li_xSi/Gr interface. As such, the predicted voltage profile and theoretical capacity exhibit close resemblance to the case of pure Si. The present work will assist in understanding the lithiation properties and performance of Si−C nanocomposites, and may provide a framework for the comparative study of various lithiated composite systems.

AUTHOR INFORMATION

Corresponding Author

*E-mail: gshwang@che.utexas.edu.

Notes

The authors declare no competing financial interest.

ACKNOWLEDGMENTS

This work was partially supported by the R.A. Welch foundation (F-1535) and SK Innovation. We would like to thank the Texas Advanced Computing Center for use of their computing resources.

REFERENCES

(1) Sharma, R. A.; Seefurth, R. N. Thermodynamic Properties of the Lithium-Silicon System. *J. Electrochem. Soc.* **1976**, *123*, 1763−1768.
(2) Boukamp, B. A.; Lesh, G. C.; Hggins, R. A. All-Solid Lithium Electrodes with Mixed-Conductor Matrix. *J. Electrochem. Soc.* **1981**, *128*, 725−729.
(3) Netz, A.; Huggins, R. A.; Weppner, W. The Formation and Properties of Amorphous Silicon as Negative Electrode Reactant in Lithium Systems. *J. Power Sources* **2003**, *95*, 119−121.
(4) Bourderau, S.; Brousse, T.; Schleich, D. M. Amorphous Silicon as A Possible Anode Material for Li-Ion Batteries. *J. Power Sources* **1999**, *81−82*, 233−236.
(5) Hatchard, T. D.; Dahn, J. R. In Situ XRD and Electrochemical Study of the Reaction of Lithium with Amorphous Silicon. *J. Electrochem. Soc.* **2004**, *151*, A838−A842.
(6) Gao, B.; Sinha, S.; Fleming, L.; Zhou, O. Alloy Formation in Nanostructured Silicon. *Adv. Mater.* **2001**, *31*, 816−819.
(7) Graetz, J.; Ahn, C. C.; Yazami, R.; Fultz, B. Highly Reversible Lithium Storage in Nanostructured Silicon. *Electrochem. Solid-State Lett.* **2003**, *6*, A194−A197.
(8) Chan, C. K.; Peng, H.; Liu, G.; McIlwrath, K.; Zhang, X. F.; Huggins, R. A.; Cui, Y. High Performance Lithium Battery Anode Using Silicon Nanowires. *Nat. Nanotechnol.* **2008**, *3*, 31−35.
(9) Beaulieu, L. Y.; Hewitt, K. C.; Turner, R. L.; Bonakdarpour, A.; Abdo, A. A.; Christensen, L.; Eberman, K. W.; Krause, L. J.; Dahn, J. R. The Electrochemical Reaction of Li with Amorphous Si-Sn Alloys. *J. Electrochem. Soc.* **2003**, *150*, A149−A156.
(10) Mao, O.; Turner, R. L.; Courtney, I. A.; Fredericksen, B. D.; Buckett, M. I.; Krause, L. J.; Dahn, J. R. Active/Inactive Nanocomposites as Anodes for Li-Ion Batteries. *Electrochem. Solid-State Lett.* **1999**, *2*, 3−5.
(11) Fleischauer, M. D.; Topple, J. M.; Dahn, J. R. Combinatorial Investigations of Si-M (M = Cr + Ni, Fe, Mn) Thin Film Negative Electrode Materials. *Electrochem. Solid-State Lett.* **2005**, *8*, A137−A140.

(12) Ghassemi, H.; Au, M.; Chen, N.; Heiden, P. A.; Yassar, R. S. In-Situ Lithiation/Delithiation Observation of Individual Amorphous Si Nanorods. *ACS Nano* **2011**, *5*, 7805−7811.
(13) Yang, J.; Winter, M.; Besenhard, J. O. Small Particle Size Multiphase Li-Alloy Anodes For Lithium-Ion-Batteries. *Solid State Ionics* **1996**, *90*, 281−284.
(14) Huggins, R. A.; Nix, W. D. Decrepitation Model For Capacity Loss During Cycling of Alloys in Rechargeable Electrochemical Systems. *Ionics* **2000**, *6*, 57−63.
(15) Li, J.; Dozier, A. K.; Li, Y.; Yang, F.; Cheng, Y. -T. Crack Pattern Formation in Thin Film Lithium-Ion Battery Electrodes. *J. Electrochem. Soc.* **2011**, *158*, A689−A694.
(16) Feng, X.; Yang, J.; Gao, P.; Wang, J.; Nuli, Y. Facile Approach To An Advanced Nanoporous Silicon/Carbon Composite Anode Material For Lithium Ion Batteries. *RSC Adv.* **2012**, *2*, 5701−5706.
(17) Wang, C. M.; Li, X.; Wang, Z.; Xu, W.; Liu, J.; Gao, F.; Kovarik, L.; Zhang, J. -G.; Howe, J.; Burton, D. J.; Liu, Z.; Xiao, X.; Thevuthasan, S.; Baer, D. R. In Situ TEM Investigation of Congruent Phase Transition and Structural Evolution of Nanostructured Silicon/Carbon Anode For Lithium Ion Batteries. *Nano Lett.* **2012**, *12*, 1624−1632.
(18) Howe, J. Y.; Burton, D. J.; Qi, Y.; Meyer, H. M., III; Nazri, M.; Nazri, G. A.; Palmer, A. C.; Lake, P. D. Improving Microstructure of Silicon/Carbon Nanofiber Composites as A Li Battery Anode. *J. Power Sources* **2013**, *221*, 455−461.
(19) Lai, J.; Guo, H.; Wang, Z.; Li, X.; Zhang, X.; Wu, F.; Yue, P. Preparation and Characterization of Flake Graphite/Silicon/Carbon Spherical Composite as Anode Materials For Lithium-Ion Batteries. *J. Alloys Compd.* **2012**, *530*, 30−35.
(20) Song, T.; Lee, D. H.; Kwon, M. S.; Choi, J. M.; Han, H.; Doo, S. G.; Chang, H.; Park, W. I.; Sigmund, W.; Kim, H.; Paik, U. Silicon Nanowires With a Carbon Nanofiber Branch as Lithium-Ion Anode Material. *J. Mater. Chem.* **2011**, *21*, 12619−12621.
(21) Li, Y.; Guo, B.; Ji, L.; Lin, Z.; Xu, G.; Liang, Y.; Zhang, S.; Toprakci, O.; Hu, Y.; Alcoutlabi, M.; Zhang, X. Structure Control and Performance Improvement of Carbon Nanofibers Containing a Dispersion of Silicon Nanoparticles For Energy Storage. *Carbon* **2013**, *51*, 185−194.
(22) Wang, J. W.; Liu, X. H.; Zhao, K.; Palmer, A.; Patten, E.; Burton, D.; Mao, S. X.; Suo, Z.; Huang, J. Y. Sandwich-Lithiation and Longitudinal Crack in Amorphous Silicon Coated on Carbon Nanofibers. *ACS Nano* **2012**, *6*, 9158−9167.
(23) Klankowski, S. A.; Rojeski, R. A.; Cruden, B. A.; Liu, J.; Wu, J.; Li, J. A High-Performance Lithium-Ion Battery Anode Based on the Core−Shell Heterostructure of Silicon-Coated Vertically Aligned Carbon Nanofibers. *J. Mater. Chem. A.* **2013**, *1*, 1055−1064.
(24) Li, W.; Yang, R.; Wang, X.; Wang, T.; Zheng, J.; Li, X. Intercalated Si/C Films as The Anode for Li-Ion Batteries with Near Theoretical Stable Capacity Prepared by Dual Plasma Deposition. *J. Power Sources* **2013**, *221*, 242−246.
(25) Evanoff, E.; Magasinski, A.; Yang, J.; Yushin, G. Nanosilicon-Coated Graphene Granules as Anodes for Li-Ion Batteries. *Adv. Energy Mater.* **2011**, *1*, 495−498.
(26) He, Y. -S.; Gao, P.; Chen, J.; Yang, X.; Liao, X. -Z.; Yang, J.; Ma, Z. -F. A Novel Bath Lily-Like Graphene Sheet-Wrapped Nano-Si Composite as A High Performance Anode Material for Li-Ion Batteries. *RSC Adv.* **2011**, *1*, 958−960.
(27) Luo, J.; Zhao, X.; Wu, J.; Jang, H. D.; Kung, H. H.; Huang, J. Crumpled Graphene-Encapsulated Si Nanoparticles for Lithium Ion Battery Anodes. *J. Phys. Chem. Lett.* **2012**, *3*, 1824−1829.
(28) Gohier, A.; Laïk, B.; Kim, K. -H.; Maurice, J. -L.; Pereira-Ramos, J. -P.; Cojocaru, C. S.; Van, P. T. High-Rate Capability Silicon Decorated Vertically Aligned Carbon Nanotubes for Li-Ion Batteries. *Adv. Mater.* **2012**, *24*, 2592−2597.
(29) Magasinki, A.; Dixon, P.; Hertzberg, B.; Kvit, A.; Ayala, J.; Yushin, G. High-Performance Lithium-Ion Anodes Using A Hierarchical Bottom-Up Approach. *Nat. Mater.* **2010**, *9*, 353−358.
(30) Chevrier, V. L.; Zwanziger, J. W.; Dahn, J. R. First Principles Study of Li-Si Crystalline Phases: Charge Transfer, Electronic Structure, and Lattice Vibrations. *J. Alloys Compd.* **2010**, *496*, 25−36.
(31) Chan, M. K. Y.; Wolverton, C.; Greeley, J. P. First Principles Simulations of the Electrochemical Lithiation and Delithiation of Faceted Crystalline Silicon. *J. Am. Chem. Soc.* **2012**, *134*, 14362−14374.
(32) Chevrier, V. L.; Dahn, J. R. First Principles Model of Amorphous Silicon Lithiation. *J. Electrochem. Soc.* **2009**, *156*, A454−A458.
(33) Chevrier, V. L.; Dahn, J. R. First Principles Studies of Disordered Lithiated Silicon. *J. Electrochem. Soc.* **2010**, *157*, A392−A398.
(34) Zhang, Q.; Zhang, W.; Wan, W.; Cui, Y.; Wang, E. Lithium Insertion In Silicon Nanowires: An ab Initio Study. *Nano Lett.* **2010**, *10*, 3243−3249.
(35) Chan, T. -L.; Chelikowsky, J. R. Controlling Diffusion of Lithium in Silicon Nanostructures. *Nano Lett.* **2010**, *10*, 821−825.
(36) Zhang, Q.; Cui, Y.; Wang, E. Anisotropic Lithium Insertion Behavior in Silicon Nanowires: Binding Energy, Diffusion Barrier, and Strain Effect. *J. Phys. Chem. C* **2011**, *115*, 9376−9381.
(37) Valencia, F.; Romero, A. H.; Ancilotto, F.; Silvestrelli, P. L. Lithium Adsorption on Graphite from Density Functional Theory Calculation. *J. Phys. Chem. B* **2006**, *110*, 14832−14841.
(38) Persson, K.; Hinuma, Y.; Meng, Y. S.; der Ven, A. V.; Ceder, G. Thermodynamic and Kinetic Properties of the Li-Graphite System from First-Principles Calculations. *Phys. Rev. B* **2010**, *82*, 125416−−9.
(39) Khantha, M.; Cordero, N. A.; Molina, L. M.; Alonso, J. A.; Girifalco, L. A. Interaction of Lithium with Graphene: An Ab Initio Study. *Phys. Rev. B* **2004**, *70*, 125422−1−−8.
(40) Chan, K. T.; Neaton, J. B.; Cohen, M. L. First-Principles Study of Metal Adatom Adsorption on Graphene. *Phys. Rev. B* **2008**, *77*, 235430−−12.
(41) Zheng, J.; Ren, Z.; Guo, P.; Fang, L.; Fan, J. Diffusion of Li^+ Ion on Graphene: A DFT Study. *Appl. Surf. Sci.* **2011**, *258*, 1651−1655.
(42) Garay-Tapia, A. M.; Romero, A. H.; Barone, V. Lithium Adsorption on Graphene: From Isolated Adatoms to Metallic Sheets. *J. Chem. Theory Comput.* **2012**, *8*, 1064−1071.
(43) Fan, X.; Zheng, W. T.; Kuo, J.-L. Adsorption and Diffusion of Li Ion on Pristine and Defective Graphene. *ACS Appl. Mater. Interfaces* **2012**, *4*, 2432−2438.
(44) Blöchl, P. E. Projector Augmented-Wave Method. *Phys. Rev. B* **1994**, *50*, 17953−17979.
(45) Kresse, G.; Hafner, J. Ab Initio Molecular Dynamics for Liquid Metals. *J. Phys. Rev. B* **1993**, *47*, 558−561.
(46) Kresse, G.; Furthmuller, J. Efficiency of Ab-Initio Total Energy Calculations for Metals . and Semiconductors Using A Plane-Wave Basis Set. *Comput. Mater. Sci.* **1996**, *6*, 15−50.
(47) Kresse, G.; Furthmuller, J. Efficient Iterative Schemes for Ab Initio Total-Energy Calculations Using A Plane-Wave Basis Set. *J. Phys. Rev. B* **1996**, *54*, 11169−11186.
(48) Bostwick, A.; McChesney, J.; Ohta, T.; Rotenberg, E.; Seyller, T.; Horn, K. Experimental Studies of the Electronic Structure of Graphene. *Prog. Surf. Sci.* **2009**, *84*, 380−413.
(49) Kim, H.; Chou, C. -Y.; Ekerdt, J. G.; Hwang, G. S. Structure and Properties of Li-Si Alloys: A First-Principles Study. *J. Phys. Chem. C* **2011**, *115*, 2514−2521.
(50) Monkhorst, H. J.; Pack, J. D. Special Points for Brillouin-Zone Integrations. *Phys. Rev. B* **1976**, *13*, 5188−5192.
(51) Henkelman, G.; Arnaldsson, A.; Jonsson, H. A Fast and Robust Algorithm for Bader Decomposition of Charge Density. *Comput. Mater. Sci.* **2006**, *36*, 354−360.
(52) Peak, E.; Pak, A. J.; Hwang, G. S. A Computational Study of the Interfacial Structure and Capacitance of Graphene in [BMIM][PF_6] Ionic Liquid. *J. Electrochem. Soc.* **2013**, *160*, A1−A10.
(53) Zhang, T.; Fu, L.; Gao, J.; Yang, L.; Wu, Y.; Wu, H. Core-Shell Si/C Nanocomposite as Anode Material for Lithium Ion Batteries. *Pure Appl. Chem.* **2006**, *78*, 1889−1896.

(54) Kauzlarich, S. M. *Chemistry, Structure, and Bonding of Zintl Phases and Ions*; Wiley−VCH Publishers: New York, 1996.